Performance Comparisons of Continuous Miniature Crystal Element (cMiCE) Detectors

Tao Ling, *Student Member, IEEE*, Kisung Lee, and Robert S. Miyaoka, *Member, IEEE*

***Abstract*—In this paper, we investigated the performance characteristics of continuous miniature crystal element (cMiCE) detectors. Versions with a 25 mm by 25 mm by 4 mm-thick LSO crystal and with a 50 mm by 50 mm by 8 mm-thick LYSO crystal were evaluated. Both detectors utilize a 64-channel flat panel photomultiplier tube (PMT). The intrinsic spatial resolution for the detectors was evaluated using Anger (i.e., simple centroid) positioning and a statistics based positioning (SBP) algorithm. We also compared the intrinsic spatial resolution for the 8-mm-thick LYSO crystal using different reflective materials (e.g., TFE Teflon, white paint, and a polymer mirror film) applied on the entrance surface of the crystal. The average energy resolution was 20% for the 4-mm-thick LSO crystal and ranged from 16% to 21%, depending upon reflective material, for the 8-mm-thick LYSO crystal. The average intrinsic spatial resolution for the 4-mm-thick crystal was 1.8-mm full width at half maximum (FWHM) for Anger positioning to within 3 mm of the crystal's edge and 1.14-mm FWHM for SBP to within 2 mm of the edge. The average intrinsic spatial resolution for the 8-mm-thick crystal was 2.2-mm FWHM for Anger positioning to within 8 mm of the crystal's edge and 1.3- to 1.5-mm FWHM (depending on reflective material used) for SBP to within 2 mm of the edge. Intrinsic spatial resolution is reported without correcting for point source size. The point spot flux had a FWHM of about 0.52 mm. The SBP algorithm resulted in significant improvement in intrinsic spatial resolution, linearity of positioning result, and effective field of view (FOV) for our cMiCE detector.**

***Index Terms*—Continuous crystal, position sensitive photomultiplier tube (PS-PMT), positioning algorithm, small animal PET.**

I. Introduction

DISCRETE crystal detector modules have traditionally been used to achieve high spatial resolution for small animal positron emission tomography (PET) scanners [1]. However, cost goes up considerably as one uses a smaller and smaller cross-section crystal. We have previously investigated a continuous miniature crystal element (cMiCE) detector that comprised a 25 mm by 25 mm by 4 mm-thick slab of LSO coupled to a 26-mm square, cross-anode position sensitive photomultiplier tube (PMT) (Hamamatsu R5900-00-C12, Japan) as a lower cost alternative to high resolution discrete crystal designs [2]. In that work, we introduced a statistics-based positioning (SBP) algorithm, similar to previously proposed maximum-likelihood (ML) methods [3]–[5], which improved the positioning characteristics near the edge of the crystal. We now investigate the performance characteristics using a 52-mm square, 64-channel flat panel PMT (Hamamatsu H8500, Japan). Experimental results were acquired along one axis of the detectors for a 25 mm by 25 mm by 4 mm-thick slab of LSO (CTI, Knoxville, TN) and a 50 mm by 50 mm by 8 mm-thick slab of LYSO (Saint Gobain, Newbury, OH).

The overall goal of this work is to develop a continuous crystal detector module with ~1.2-mm full width at half maximum (FWHM) intrinsic spatial resolution and adequate detection efficiency for *in vivo* small animal imaging. We investigate the intrinsic spatial resolution of a detector module using our SBP method, as the crystal thickness increases from 4 to 8 mm. The primary reason for loss of spatial resolution for thicker detectors is the depth dependence of the detector's light response function. For a 9.5-mm-thick NaI(Tl) gamma camera, the depth of interaction (DOI) can account for a 6.4-mm discrepancy in position [6]. Additional reasons for loss of spatial resolution as the crystal gets thicker are broadening of the light response function, more Compton scatter in the crystal and a larger fraction of the crystal being influenced by edge effects. In this work, we also study the effect the reflective material used on the entrance surface of the crystal (opposite the PMT) has on intrinsic spatial resolution.

II. Material and Methods

Each of the crystals was similarly fabricated. The two large area surfaces were polished and the edges were left as cut (or slightly roughened). The roughened edges were painted black to reduce reflected light. The crystals were coupled to the PMT using Bicron BC-630 optical grease (Saint Gobain, Newbury, OH). The surface of the crystal opposite the PMT was backed with TFE Teflon, mirror film reflector (3 M, St Paul, MN) or painted white (Rust-Oleum, Vermont Hills, IL).

A. Statistics Based (ML) Positioning Algorithm [2]

Suppose, the distributions of observing PMT outputs $\mathrm{M} = \mathrm{M}_1, \mathrm{M}_2, \ldots, \mathrm{M}_\mathrm{n}$ for scintillation position x, are independent normal distributions with mean, $\mu(\mathrm{x})$, and standard deviation $\sigma(\mathrm{x})$.

The likelihood function for making any single set of observations $\{\mathrm{m_i}\}$ from distributions $\{\mathrm{M_i}\}$ given x is

$$L[m_i|x] = \prod_{i=1}^{n} \frac{1}{\sigma_i(x)\sqrt{2\pi}} \exp\left(-\frac{(m_i - \mu(x))^2}{2\sigma_i^2 x}\right).$$

Manuscript received February 27, 2006. This work was supported in part by the NIH-NIBIB by Grants R21 EB001563 and R01 EB002117.

T. Ling is with the Department of Physics, University of Washington, Seattle, WA 98195 USA (e-mail: lingtop@u.washington.edu).

K. Lee was with the University of Washington, Seattle, WA 98195 USA. He is now with the Department of Electrical Engineering, Kongju National University, Korea (e-mail: klee@kongju.ac.kr).

R. S. Miyaoka is with the Radiology Department, University of Washington, Seattle, WA 98195 USA (e-mail: rmiyaoka@u.washington.edu).

Digital Object Identifier 10.1109/TNS.2006.882296

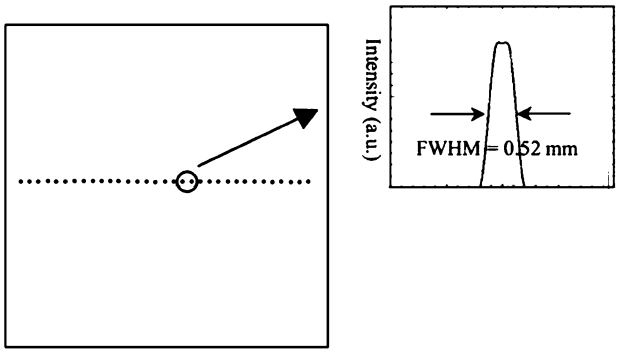

Fig. 1. Point fluxes (black dots) are along one axis across the center of crystal (square). Profile of point flux is shown in inset, it has a FWHM of 0.52 mm.

The maximum likelihood estimator of the event position x is given by

$$\hat{x} = \arg\min_{x} \left[\sum_{i} \frac{(m_i - \mu_i(x))^2}{2\sigma_i^2(x)} \right].$$

B. Detector Calibration

For each of the crystals data were collected for point spot fluxes at locations with 1-mm interval along the *X* axis of the crystal as illustrated in Fig. 1. The point spot flux was produced using a 0.25-mm diameter, 23 μCi Na-22 source (Isotope Products, Valencia, CA) and a 2 mm by 2 mm cross-section coincidence detector placed at a distance from the source. Based upon the geometry of the setup, the point spot flux had a square shape and a FWHM of $\sim$0.52 mm as illustrated in Fig. 1.

All 64 channels from the multianode, flat panel PMT were acquired for each coincidence event. Two 32-channel CAEN ADC cards (N792 ADCs, CAEN, Italy) were used as part of a VME data acquisition system. The VME crate was connected to an Apple computer running OS X and the Orca software package [7] using a VME-PCI adapter card.

C. Data Filtering

The basis of our SBP method is an accurate characterization of the light distribution functions versus interaction position in the crystal. In the ideal experimental situation the SBP look up tables would be generated from events that have undergone a single photoelectric interaction in the crystal. However, $\sim$61% of the first interactions in lutetium-based scintillators are Compton scatter. Therefore, we developed a two-step data filtering technique that we apply to our raw data to preferentially select the data we use to build our SBP look up tables. In the first step, we set an energy window of $\pm$20% around the photopeak to select 511-keV events that were photoelectrically absorbed in the crystal, as shown in Fig. 2. Second, we used an "Anger mask" technique to reduce the number of events used for the light response characterization that Compton scatter before being photoelectrically absorbed. Events within the photopeak energy window were positioned using Anger logic. A mask with radius of 1 standard deviation around the center as illustrated in Fig. 3, was applied. Events within the mask were most likely single photoelectric absorption events and kept for look-up table (LUT) building. By using an "Anger mask," we were able to eliminate a good fraction of the events with multiple interactions within the crystal from biasing the true relationship between the photon interaction location and the light distribution.

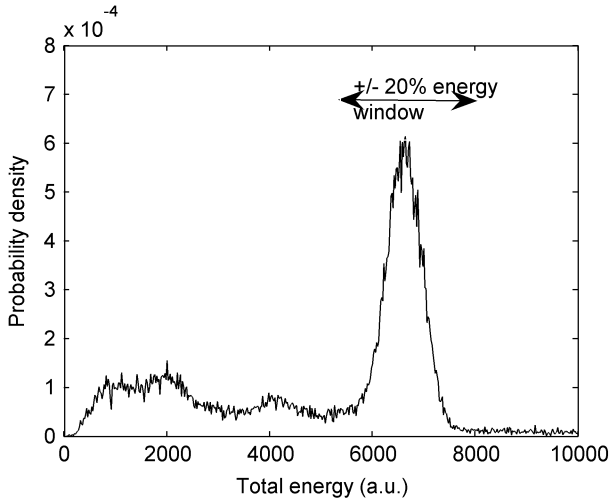

Fig. 2. Energy window of $\pm 20\%$ around the photopeak.

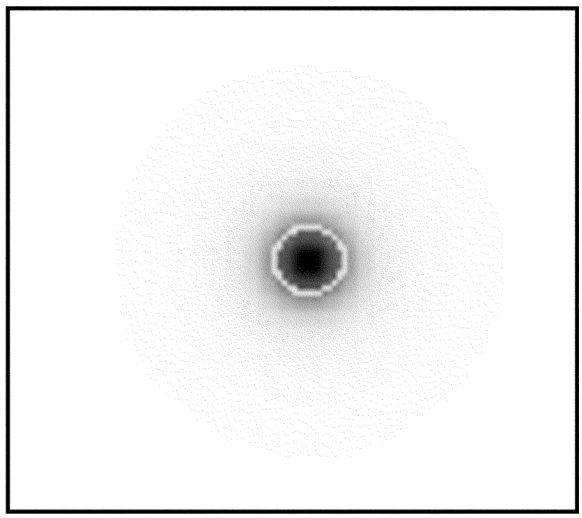

Fig. 3. Point source using Anger positioning. Only points within the light "Anger mask" circle are used for SBP look up table generation.

Two one-dimensional (1-D) LUTs (i.e., the mean and standard deviation of the light collection histogram for each channel versus spot position) were generated for SBP, based on the filtered data sets. Typical light response functions (LRF) are shown in Fig. 4. Note that the full width half maximum of the light response function for the 4-mm-thick crystal is $\sim$9 mm and for the 8-mm-thick crystal is $\sim$14 mm. Even though SBP could only be used in one dimension, all 64 channels of information were used to position each event.

D. Performance Evaluation

Performance of the cMiCE detector was examined with a testing data set that was different from the data used for char-

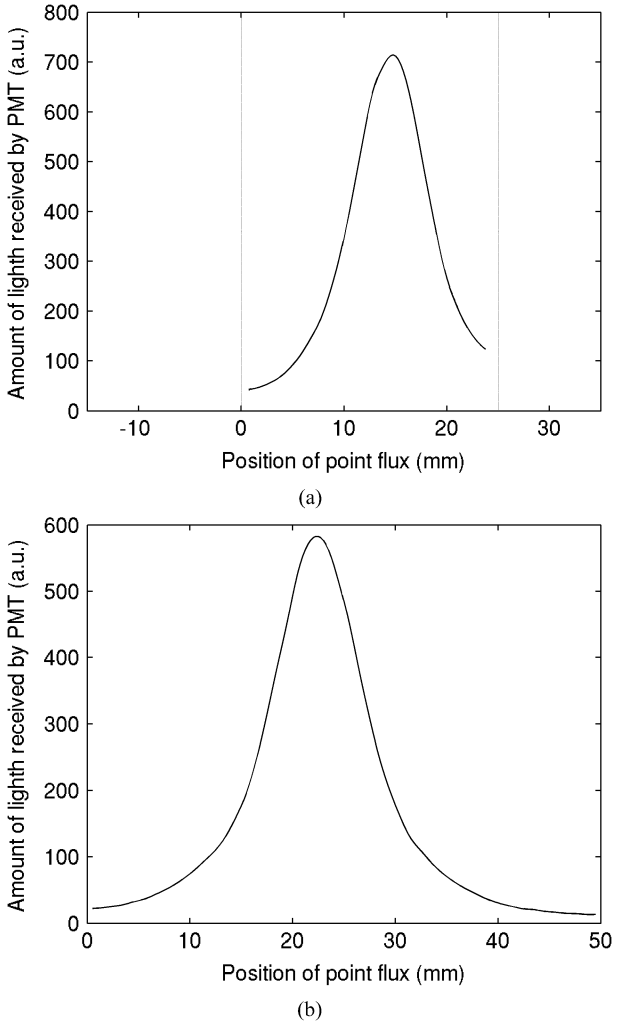

Fig. 4. Typical LRF for (a) 4– ; (b) 8–mm-thick crystal with Teflon. (LRFs for white paint or mirror film are similar to the above.)

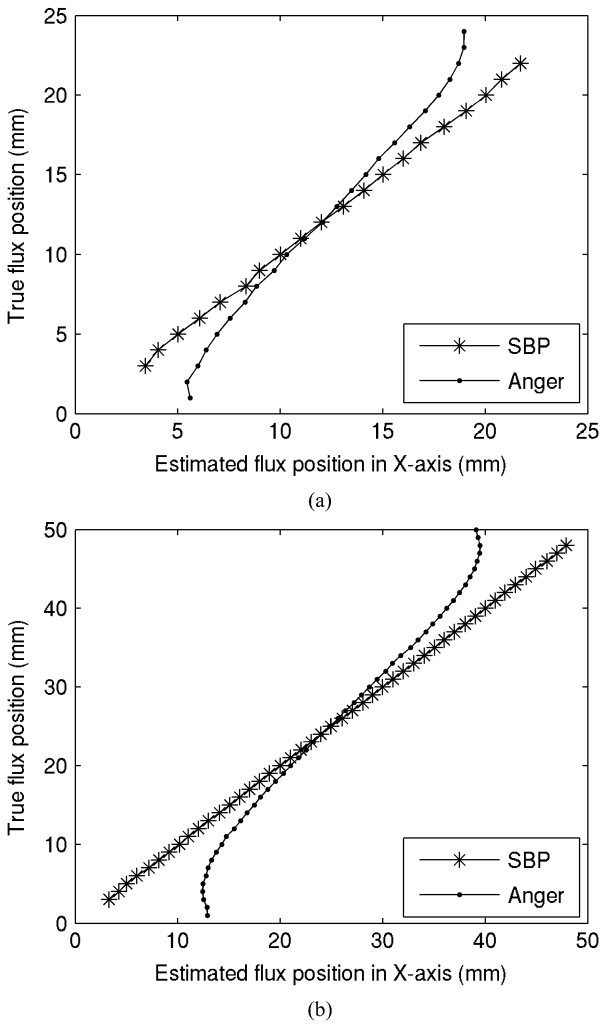

Fig. 5. Linearity correction curve for (a) 4- ; (b) 8-mm cMiCE detector.

acterization. An energy window was applied to the testing data set.

For SBP data were positioned using an exhaustive search algorithm along the direction (i.e., the *X* axis) the characterization data were collected. To generate a two-dimensional (2-D) point spread function (PSF), we positioned each event in Y using Anger positioning. For comparison purposes, data were also positioned in both *X* and *Y* axis using Anger positioning by calculating the simple centroid. Both results were corrected for nonlinearity afterward. The linearity correction curve was shown in Fig. 5. The intrinsic spatial resolution was determined by fitting a Gaussian curve to the *X*-axis profile through the peak of the 2-D PSF after correction, as shown in Fig. 6.

III. Results

A. Comparison of 4- and 8-mm-Thick Crystals

Results using TFE Teflon on the entrance surface of the crystal are provided for both the 4- and 8-mm-thick crystal detectors. The average spatial resolution without correcting for source size was 1.80.5-mm FWHM for the 4-mm-thick crystal (to within 3 mm of the crystal's edge) and 2.20.7-mm FWHM for the 8-mm crystal (to within 8 mm of the crystal's edge) using Anger (i.e., simple centroid) positioning.

For SBP the measured intrinsic spatial resolution was 1.14 ± 0.17 mm, and 1.4 ± 0.3 mm for 4- and 8-mm crystals (to within 2 mm of the crystal's edge for both), respectively. The spatial resolutions from different positioning methods versus flux position are plotted in Fig. 7(a) and (b).

The useful field of view (FOV) along the center of the crystal using SBP was approximately 21 and 46 mm for the 4- and 8-mm-thick cMiCE detectors, respectively. Using simple centroid positioning, it was less than 19 and 34 mm, respectively.

The average energy resolution was 20% for the 4-mm-thick and 21% for the 8-mm-thick crystal detectors.

Two-dimensional contour plots of the SBP positioning results for the 4- and 8-mm-thick detectors of several point fluxes spaced 2 mm apart across the detectors are illustrated in Fig. 8. The contours representing the FWHM of the point response functions are shown in the plots.

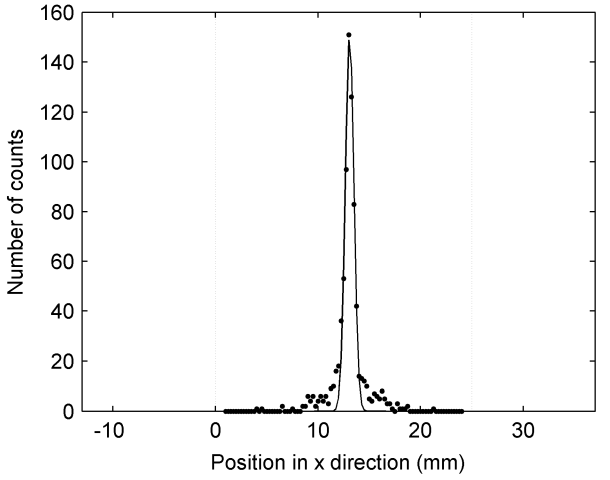

(a)

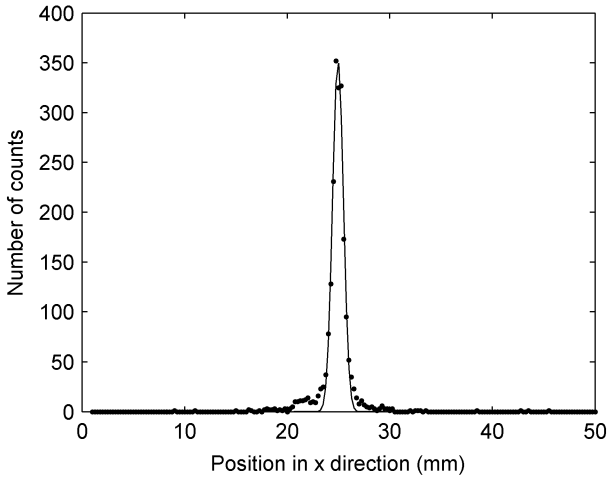

(b)

Fig. 6. Profiles of SBP results (dots) along x direction and their Gaussian fit (curve); from the central section of (a) 4-mm-thick crystal, $\mathrm{x} = 13$ mm, $\mathrm{FWHM} = 0.97$ mm. (b) 8-mm-thick crystal with Teflon, $\mathrm{x} = 25$ mm, $\mathrm{FWHM} = 1.2$ mm.

B. Comparison of Different Reflective Materials (8-mm-Thick Crystal)

Results using different reflective materials on the entrance surface of the 8-mm-thick crystal are listed in Table I. White paint had the best energy resolution and the best spatial resolution using SBP. TFE Teflon had the best spatial resolution using Anger positioning. Based upon these results, the white paint provided the best overall performance.

C. Estimated Coincidence Response Functions

Coincidence response functions (CRF) were generated by convolving the 1-D intrinsic spatial resolution profile along the *X* axis (as in Fig. 6) with itself. Results are illustrated in Fig. 9. The profile of the CRF was fit to a Gaussian and the FWHM is reported as the spatial resolution of the detector. The results indicate that the tails of the intrinsic spatial resolution will not significantly broaden FWHM coincidence resolution for a system using our cMiCE detectors.

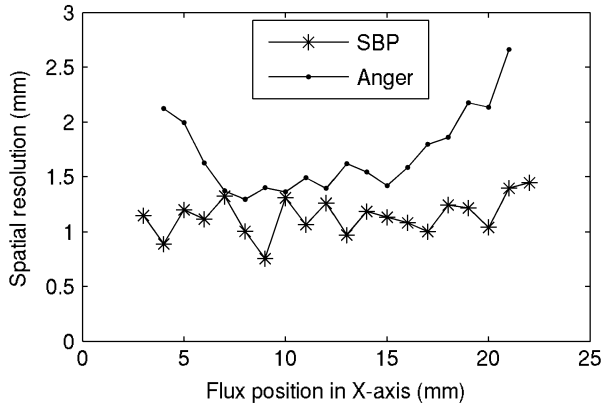

(a)

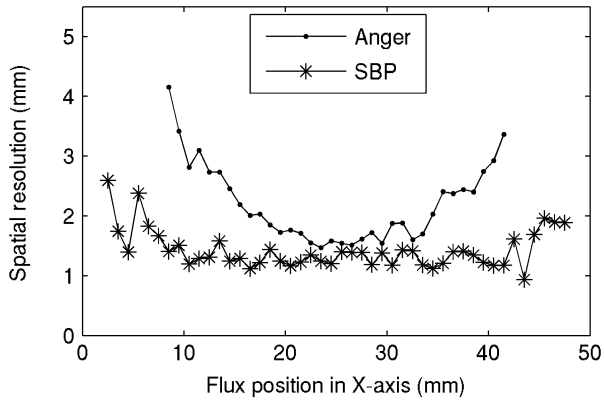

(b)

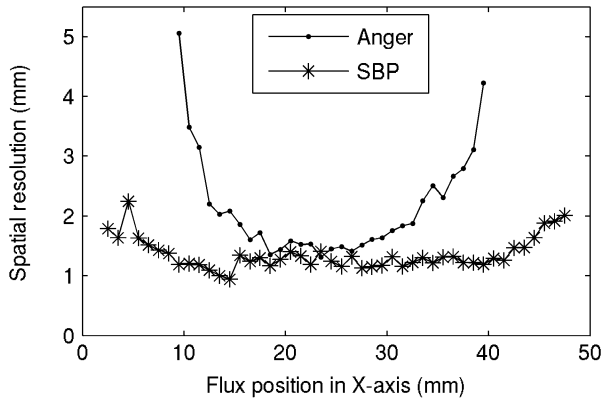

(c)

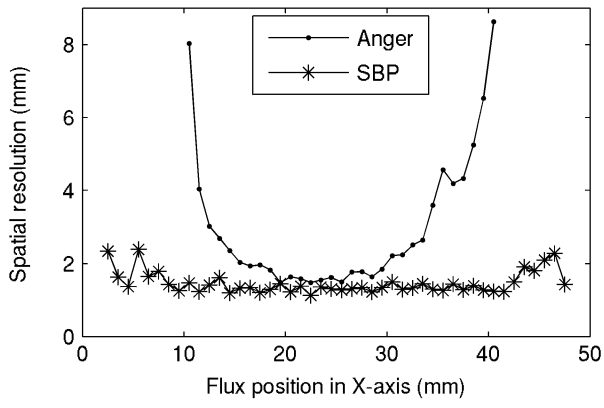

(d)

Fig. 7. Spatial resolutions using SBP and simple centroid algorithm of (a) 4-mm; (b)–(d) 8-mm-thick crystal with Teflon, white paint, or mirror film.

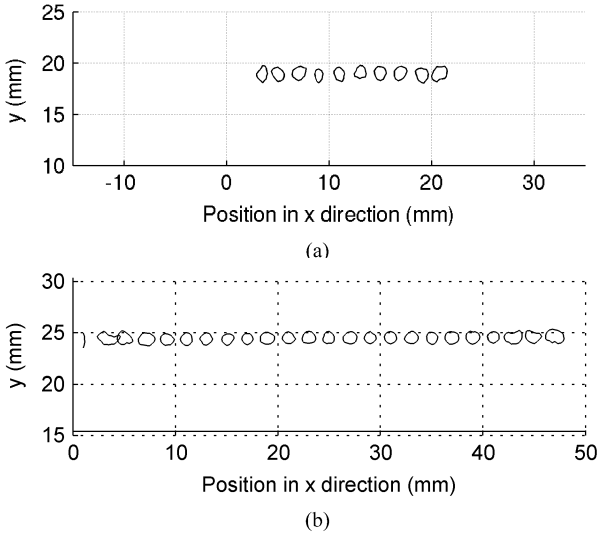

Fig. 8. FWHM contour plots of PSF from SBP with 2-mm spacing for the (a) 4- ; (b) 8-mm-thick crystals with TFE Teflon reflector.

TABLE I
COMPARISON OF DIFFERENT REFLECTIVE MATERIALS

Material	Energy resolution	Anger Intrinsic spatial resolution (mm)	SBP Intrinsic spatial resolution (mm)
Teflon	21%	2.2 ± 0.7	1.4 ± 0.3
White paint	16%	2.6 ± 1.7	1.3 ± 0.3
Mirror film	21%	3.4 ± 2.6	1.5 ± 0.3

TABLE II
ESTIMATED COINCIDENCE RESOLUTIONS FOR DIFFERENT cMiCE DETECTOR PAIRS

Crystal/Reflective material	Average coincidence resolution (mm)
4mm LSO/Teflon	1.01± 0.12
8mm LSO/Teflon	1.22± 0.21
8mm LSO/White paint	1.18± 0.26
8mm LSO/Mirror film	1.30± 0.24

IV. DISCUSSION AND CONCLUSION

As expected, the intrinsic spatial resolution for our continuous crystal detector module increased going from a 4-mm-thick crystal (1.14 ± -0.17 mm FWHM) to an 8-mm-thick crystal (1.4 ± -0.3-mm FWHM). However the increase was not too significant. At 1.4-mm FWHM the 8-mm-thick detector still has excellent intrinsic spatial resolution characteristics and will provide close to a factor of three in increased coincidence detection efficiency.

We believe the two main factors for the degradation in intrinsic spatial resolution are the depth dependence of the light response function of the crystal and the broader spread of light associated with the thicker crystal. We therefore investigated whether different reflective materials on the front entrance of the crystal could improve the intrinsic spatial resolution performance versus using TFE Teflon.

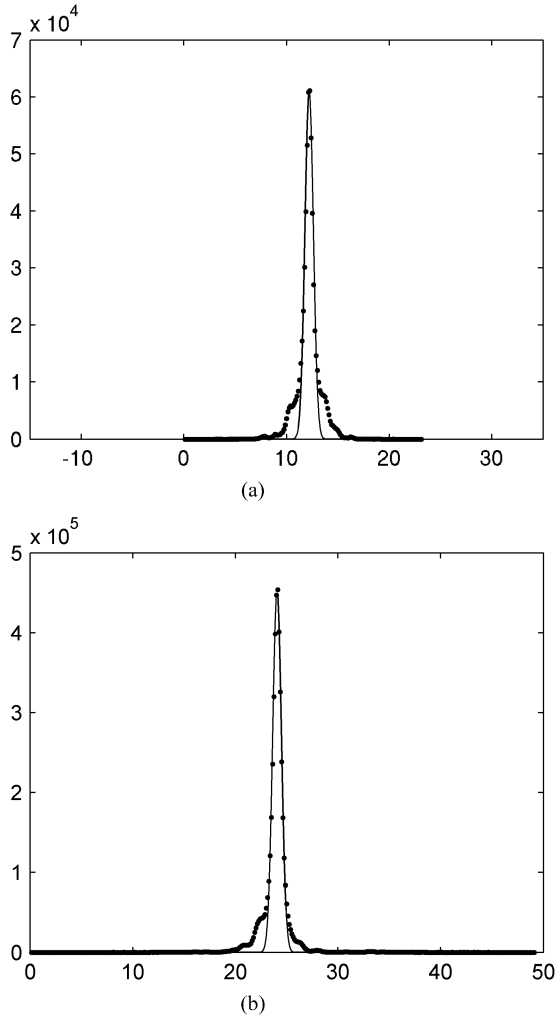

Fig. 9. Profiles of Coincidence response functions (dots) along *x* direction and their Gaussian fit (curve) for (a) 4-mm LSO and (b) 8-mm-thick LYSO cMiCE detector. The FWHMs are 0.945 and 0.978 mm, respectively.

Using Anger (i.e., simple centroid) positioning, TFE Teflon had the best intrinsic resolution, which is consistent with the conclusion from Karp and Muehllehner of using a diffuse reflector for the entrance surface of the crystal [8]. For our SBP method, white paint outperformed the other two; however, the difference was not significant. We conclude that SBP is not very sensitive to the reflectors that we used; however, intrinsic spatial resolution may be improved if different surface treatments can be used to narrow the light response function of the crystal.

The main advantages of using the SBP algorithm over the simple centroid algorithm are four fold: 1) spatial resolution, 2) spatial resolution uniformity, 3) positioning linearity, and 4) effective FOV. The drawback is that the light response functions for the detector must be fully characterized to achieve optimal performance.

Another important feature of the SBP method is that it is feasible to extend it to estimate depth of interaction. DOI capability can be implemented coherently within the ML framework, if 3-D LUTs are available. We have previously shown some promising results to derive 3-D LUTs using simulated data [9] and are extending that work to use experimental data.

Neither the Anger nor the SBP results reported here were ideal. The Anger positioning result can be improved by optimizing the weights associated with each PMT channel. For SBP, better performance would be expected when using a fully 2-D LUT, instead of using different positioning methods for the *X* and *Y* axes of the crystal.

The results of this paper illustrate that as the thickness of the crystal increases (i.e., from 4 to 8 mm), high spatial resolution can still be achieved. This demonstrates that the development of a low cost, high resolution small animal PET system with good detection efficiency is feasible.

REFERENCES

[1] M. Dahlbom and E. J. Hoffman, "An evaluation of a two-dimensional array detector for high resolution PET," *IEEE Trans. Med. Imag.*, vol. 7, no. 4, pp. 264–272, Dec. 1988.

[2] J. Joung, R. S. Miyaoka, and T. K. Lewellen, "CMiCE: A high resolution animal PET using continuous LSO with a statistics based positioning scheme," *Nucl. Instrum. Methods Phys. Res. A*, vol. 489, no. 1–3, pp. 584–589, Aug. 2002.

[3] T. D. Milster, J. N. Aarsvold, H. H. Barrett, A. L. Landesman, L. S. Mar, D. D. Patton, T. J. Roney, R. K. Rowe, and R. H. Seacat, "A full-field modular gamma camera," *J. Nucl. Med.*, vol. 31, no. 5, pp. 632–639, May 1990, 3rd.

[4] R. M. Gray and A. Macovski, "Maximum a posteriori estimation of position in scintillation cameras," *IEEE Trans. Nucl. Sci.*, vol. 23, no. 1, pp. 849–852, 1976.

[5] N. H. Clinthorne, W. L. Rogers, L. Shao, and K. F. Koral, "A hybrid maximum likelihood position computer for scintillation cameras," *IEEE Trans. Nucl. Sci.*, vol. 34, no. 1, pp. 97–101, Feb. 1987.

[6] D. Gagnon, N. Pouliot, L. Laperriere, M. Therrien, and P. Olivier, "Maximum likelihood positioning in the scintillation camera using depth of interaction," *IEEE Trans. Med. Imag.*, vol. 12, no. 1, pp. 101–107, Mar. 1993.

[7] M. A. Howe, G. A. Cox, P. J. Harvey, F. McGirt, K. Rielage, J. F. Wilkerson, and J. M. Wouters, "Sudbury neutrino observatory neutral current detector acquisition software overview," *IEEE Trans. Nucl. Sci*, vol. 51, no. 3, pt. part 3, pp. 878–883, Jun. 2004.

[8] J. S. Karp and G. Muehllehner, "Performance of a position-sensitive scintillation detector," *Phys. Med. Biol.*, vol. 30, pp. 643–655, 1985.

[9] R. S. Miyaoka and K. Lee, "Investigation of detector light response modeling for a thick continuous slab detector," in *Conf. Rec. 2004 IEEE Nucl. Sci. Symp.*, vol. 4, pp. 2479–2482.